

Phospholemman transmembrane structure reveals potential interactions with Na^+/K^+ -ATPase*

Andrew J. Beevers¹ and Andreas Kukol²

From the Department of Chemistry¹, University of Warwick, Coventry, UK
From the School of Life Sciences², University of Hertfordshire, Hatfield, UK

Running Title: Phospholemman transmembrane structure

Address correspondence to: Andreas Kukol, The School of Life Sciences, University of Hertfordshire, Hatfield AL10 9AB, UK, Tel.: +44-1223-840818; E-Mail: ak284@cam.ac.uk

Subject categories: Structural Biology, Membranes & Transport

Phospholemman (PLM) is a 72-residue bitopic cardiac transmembrane protein, which acts as a modulator of the Na^+/K^+ -ATPase, the $\text{Na}^+/\text{Ca}^{2+}$ exchanger, and possibly forms taurine channels in non-heart tissue. This work presents a high-resolution structural model obtained from a combination of site-specific infrared spectroscopy and experimentally constrained high-throughput molecular dynamics (MD) simulations. Altogether 37 experimental constraints including 9 long-range orientational constraints have been used during MD simulations in an explicit lipid bilayer/water system. The resulting tetrameric α -helical bundle has an average helix tilt of 7.3° and a crossing angle close to 0° . It does not reveal a hydrophilic pore but instead strong interactions between various residues occlude any pore. The helix-helix packing is unusual with Gly19 and Gly20 pointing to the outside of the helical bundle facilitating potential interaction with other transmembrane proteins, thus providing a structural basis for the modulatory effect of PLM on the Na^+/K^+ -ATPase. A two-stage model of interaction between PLM and the Na^+/K^+ -ATPase is discussed involving PLM-ATPase interaction and subsequent formation of an unstable PLM trimer, which readily interacts with surrounding ATPase molecules. Further unconstrained MD simulations identified other packing models of PLM, one of which could potentially undergo a conformational transition to an open pore.

Human phospholemman (PLM) is a member of a family of single-span transmembrane proteins characterised by the invariant extracellular motif FXYD (1) and is also known as FXYD1. It is found in liver, skeletal muscle and most abundantly in the cardiac sarcolemma (2). Over recent years conclusive experimental evidence has been presented that PLM acts as a tissue specific modulator of the Na^+/K^+ -ATPase similar to the other members of the FXYD family, each of which is prevalent in a different tissue, summarised in several recent reviews (3,4). The Na^+/K^+ -ATPase consists of a catalytic α -subunit with 10 transmembrane segments and a β -subunit involved in membrane insertion and as a modulator of transport properties (5). In particular cross-linking and modelling studies revealed the direct interaction between the Na^+/K^+ -ATPase α -subunit and members of the FXYD family (γ and CHIF), which involves the binding of a single transmembrane domain into a groove formed by M2, M6 and M9 transmembrane helices of the Na^+/K^+ -ATPase (6,7). PLM appears to be a major control point in the function of heart cells, although its specific physiological role is unclear, complicated by the possibility that its regulatory effect on the Na^+/K^+ -ATPase may depend on the phosphorylation state of PLM (8) as well as other less well established functional roles, e.g. interaction with the $\text{Na}^+/\text{Ca}^{2+}$ exchanger (9,10) or independent channel formation. PLM knockout mice expressed a complex response including increased cardiac mass, larger cardiomyocytes and ejection fractions in the absence of hypertension, while the overall Na^+/K^+ -ATPase activity was

reduced by 50% (11). There is growing evidence that PLM regulates the activity of Na/Ca²⁺ exchanger 1 (NCX1) from heterologous expression studies of PLM and NCX1 in HEK239 cells (10), overexpression of PLM in rat cardiomyocytes (12,13) using different approaches to measure NCX1 activity. It appears that phosphorylation of PLM abolishes its inhibitory effect on the Na⁺/K⁺-ATPase (14,15), while the phosphorylated form of PLM inhibits NCX1 (9,12).

Electrical measurements of PLM in artificial lipid bilayers and oocytes showed that PLM facilitates the membrane flux of ions (16) and taurine transport (17), which leads to the possibility that PLM has a function in the regulation of cell volume either as a modulator of a swelling-activated signal transduction pathway or directly facilitating osmolyte influx in non-cardiac tissues (18).

The three-dimensional structure of PLM is not known, but on the basis of hydropathy analysis of the amino acid sequence a transmembrane domain from residue 18 to 37 has been predicted (2) and confirmed later by attenuated total reflection (ATR) FTIR spectroscopy (19). The C-terminus is located intracellularly, resistant to protease digestion, while the N-terminus is located extracellularly as shown by antibody labelling (20). A PLM peptide of residues 12 to 39 comprising the transmembrane domain forms α -helical tetramers in lipid bilayers, which are tilted by less than 17° against the membrane normal (19). Here we present a detailed three-dimensional structure of the tetrameric transmembrane domain based on site-specific infrared dichroism (SSID) (21,22) combined with a recently developed conformational search based on experimentally constrained high-throughput molecular dynamics (MD) simulations in an explicit lipid bilayer. (23,24).

EXPERIMENTAL PROCEDURES

Preparation of Labelled Peptides – ¹³C amino acids were obtained from Cambridge Isotope Laboratories (Cambridge, MA) and further labelled by reaction with H₂¹⁸O catalysed by gaseous hydrochloric acid (25,26). The labelled amino acids were then Fmoc protected by a

standard procedure using Fmoc-N-succinimyl-carbonate (27).

Ten peptides of the transmembrane domain sequence of PLM (residues 12-39 DYQSLQIGGLVIAGILFILGILIVLSRR) were obtained from Keck Laboratories (Yale University, USA). Each peptide contains one ¹³C=¹⁸O labelled residue in the positions shown in boldface.

Preparation of Proteoliposomes – Peptides were mixed with dimyristoylphosphocholine (DMPC) lipids in hexafluoroisopropanol (HFIP) at a ratio of approx. 1:30 (w/w). Liposomes were then made by complete evaporation of the HFIP and addition of water to a lipid concentration of 10 mg/ml. The lipid suspension was then sonicated and subjected to a freeze-thaw cycle three times.

Infrared Spectroscopy – The liposome suspensions were deposited onto a trapezoidal Germanium refraction element (50 mm x 2 mm x 20 mm) and bulk water was removed under a stream of nitrogen, forming a thick film compared to the penetration depth of the IR light on the element. Attenuated total reflection (ATR) FTIR spectra were obtained using a Bruker Tensor FTIR-Spectrometer (Bruker Optics, Coventry, UK) with a high sensitivity liquid nitrogen cooled MCT/A detector. One spectrum was calculated from the average of 1000 interferograms at a resolution of 2cm⁻¹ per data point in the 4000 cm⁻¹ to 1000 cm⁻¹ range of the electromagnetic spectrum. In each case the spectra was recorded at parallel and perpendicular polarisation to the plane of incidence and the dichroic ratio was calculated as the ratio between the integrated absorption of parallel and perpendicular polarised light for the amide I absorption band centred at a wavenumber of 1658 cm⁻¹ and for the ¹³C=¹⁸O absorption band centred at 1594 cm⁻¹. For each labelled peptide, at least three independent measurements were taken.

Data Analysis – The spectra were analysed according to the theory of site-specific infrared dichroism (SSID) presented elsewhere (22,28,29). Briefly, the dichroic ratios of the amide I absorption band and the absorption band of the label for two peptides with labels in position 1 and 2 were analysed together in order to obtain the local helix tilt angle β and the rotational pitch angle ω for the label in position 1. Another peptide

with a label in position 3 was analysed in order to give the orientational parameters for position 2 and so on. In that way the following pairs of labels were analysed G20/L21, L21/V22, V22/I23, I23/G25, G25/I26, I26/L27, L27/G31, G31/I32, I32/L33.

The angle between the C=O bond and the z-axis θ_z used as orientational constraint was calculated as follows:

$\cos\theta_z = \cos\alpha\cos\beta - \sin\alpha\sin\beta\cos(\omega+17^\circ)$ with $\alpha = 180^\circ - 38^\circ = 142^\circ$ denoting the angle between the transition dipole moment and the molecular director given by Marsh et al. (30). All calculations were carried out using the Mathematica 5 software (Wolfram Research, Champaign, IL).

High Throughput Molecular Dynamics Conformational Searching – The conformational search of PLM tetrameric helical bundles were carried out as described elsewhere for a dimeric system (23,24). Briefly, α -helical bundles were generated by symmetrically rotating the helices in 10° increments in order to produce an array of starting structures for MD simulation. Both left and right-handed crossing bundles (crossing angle of $\pm 25^\circ$) were generated giving 72 different orientations, with each being simulated at four different initial random velocities resulting in a total of 288 starting structures. Each structure was subjected to 200 ps MD simulation using the GROMACS software (31) in a DMPC bilayer/water system containing 128 DMPC molecules and 3655 water molecules. The initial coordinates of the DMPC bilayer were obtained from Gurtovenko et al. (32). Constraints were placed on each α -helical bundle, the angle between the z-axis and the C=O bond of the label was constrained to the derived value from SSID. The local tilt angle was also constrained by defining the angle between the z-axis and a vector between the C α atoms of the residue in question and a residue seven positions along in the helix. Also, as the peptide is known to be α -helical (as detected from IR), the distances between hydrogen bonding pairs of amine hydrogens and carbonyl oxygens were constrained between 1.6 nm and 2.3 nm, a harmonic potential was applied outside these boundaries. All constraints were added to the GROMACS forcefield with a force constant of

5000 kJ mol⁻¹. For the unconstrained search the same procedure was followed without applying any constraints. All MD simulations were performed in parallel on an 8 node dual 2.66 GHz Xeon processor cluster (Streamline Computing, Warwick, UK).

Clustering of Structures – Ca root-mean-square-deviation (RMSD) comparisons were made between all resulting structures from the search. Structures were then clustered according to their RMSD values. The adopted criteria for structure clustering were that of a maximum RMSD value of 2 Å between two structures. For a cluster to be created, a minimum of five structures possessing RMSD values within this limit was required.

The structures contributing to this cluster were then used to create an average structure, which was subjected to experimentally constrained MD simulation for 2ns in a lipid bilayer followed by energy minimisation. The coordinates of the experimentally constrained PLM model have been deposited with the RCSB Protein Data Bank, PDB ID 2j1i.

RESULTS

ATR Infrared Spectroscopy – Altogether ten PLM transmembrane peptides containing residues 12 to 39 with ¹³C=¹⁸O labelled residues in the positions indicated in figure 1 have been reconstituted in dimiristoyl-phosphatidylcholine vesicles and analysed by polarised attenuated total reflection infrared spectroscopy. The symmetric amide I absorption band centred at approx 1658 cm⁻¹ revealed that in all cases the peptide adopted a predominantly α -helical conformation (33) confirming earlier observations (19). The absorption band of the labelled sites centred at 1594 cm⁻¹ showed that the label is also in an α -helical environment (26). In some cases a shoulder existed at 1618 cm⁻¹ (figure 1) representing the absorption of a residue with ¹³C=¹⁶O carbonyl bond, which is caused by incomplete labelling of the amino acid with H₂¹⁸O prior to peptide synthesis. However, in all cases the ¹³C=¹⁸O bond was of sufficient intensity for analysis.

The dichroic ratio of the amide I peak varied from 2.5 to 4.2, depending on sample order; whilst the dichroic ratio of the ¹³C=¹⁸O peak varied from 2.1

to 5.8, depending on position and sample order. The dichroic ratio of the label is in all cases different from the dichroic ratio of the unlabelled amide I peak, which is indicative of oligomerisation. A label in a monomeric helix would adopt an average dichroic ratio similar to the unlabelled residues due to rotational symmetry with respect to the membrane normal. The local helix tilt shows variation between $(3\pm 4)^\circ$ and $(10\pm 4)^\circ$, while the change in rotational pitch angle ω is in the region of 100° for successive residues in accordance with α -helical geometry (table 1). The angle between the C=O bond and the z-axis, calculated from ω and β , are used as experimental constraints for the MD simulation.

Constrained High-Throughput MD – At each stage of the MD simulation and energy minimisation a total of 37 experimental constraints have been applied composed of nine orientational constraints obtained from SSID of ten labelled peptides (table 1), in order to set the local helix tilt and distance constraints between the carbonyl oxygen of residue n and the amide hydrogen of residue n+4 in order to maintain the experimentally determined α -helical geometry, although unconstrained simulations of helices in lipid bilayers have shown that α -helices are retained even after long term MD simulations (23,24). Following the MD simulation of 72 different starting structures each at four different random initial atom velocities (288 simulations), a cluster analysis provided six structures (figure 2). Of these, structure 6 showed the closest agreement with the rotational pitch angles obtained from SSID experiments (table 2), even though structure 6 was of slightly higher energy than other structures. It is generally accepted that similarity to experimental studies is a far more accurate determinant than force-field energy.

Structure 6 is a right-handed α -helical bundle with a crossing angle close to 0° , whilst local helix tilt angles derived from the IR data vary from 2.5° to 10.1° depending on the site in question, resulting in an average tilt angle of 7.3° . This is in accordance with previous conventional ATR-FTIR experiments, which indicated an average tilt angle between 0° and 17° (19), if the sample order is not taken into account.

In the transmembrane region, the residues in the helices adopt α -helix geometry throughout, but close to the termini some are locally distorted. This region does not possess any constraints and therefore this effect is most likely due to the greater freedom of movement these residues will have. The centre of structure 6 is occluded by interactions between residues Tyr27, Gln31, Leu35, Phe42, Ile46, Leu50 and Arg53.

Unconstrained High-Throughput MD – In order to explore the range of all possible packing models of PLM in lipid bilayers, we performed a high-throughput MD search without any constraints applied. In this simulation we found 9 clusters of structures and calculated an average structure for each cluster (fig. 5A). The starting structure for the helix rotation $\phi = 0^\circ$ is the same as shown in fig. 2B. Each cluster average structure reveals a well packed α -helical tetramer. In order to find a model, which would support the experiments of PLM ion channel activity, we analysed visually each structure for the possibility of the formation of a hydrophilic pathway through the centre of the tetramer. For most structures the centre of the tetramer is completely occluded by interactions between several residues, but in structure number 4 only the side-chains of Val34 and Tyr27 occlude the centre of the structure as shown in fig. 5B, while other side-chains are either pointing to the outside or are involved in close packing interaction at the helix-helix interface. Tyr27 is located in the water phase at the N-terminal end of the peptide and shows a high conformational flexibility in MD simulations, thus would not contribute significantly to occlusion of the pore, while Val34 is located in the transmembrane domain. Structure number 4 has the lowest energy of all unconstrained packing models of -1299 kJ, while the next lowest energy structure is structure 3 with -1253 kJ.

DISCUSSION

Constrained High-throughput MD simulation – The conformational search combining MD simulations in a realistic environment with long-range orientational constraints allowed us to obtain an experimentally defined structural model of the PLM tetrameric transmembrane domain with atomic detail.

However, a comparison of the rotational pitch angles between the experiment and the best model structure 6 reveals some deviations (table 2). This is caused on the one hand by the interplay between the experimental constraints and the tendency of the structure to adopt an energy minimum in the “imperfect” computational forcefield, which also takes into account side chain packing and protein-lipid interaction for which we have no experimental data. On the other hand, the rotational pitch angle for a residue is a derived parameter assuming ideal α -helix geometry, which is not the case for PLM and other helices, thus calculation of this angle leads to deviations, while the angles between the C=O bond and the z-axis used as actual constraints in the simulation were matched precisely (data not shown). However, as the rotational pitch angle of a residue defines the interaction side of helices in a bundle, comparisons based on this angle have been proven most reliable even allowing the determination of the preferred oligomerisation state (34).

PLM as Na⁺/K⁺-ATPase regulator – PLM has three regions of its transmembrane sequence conserved in human, canine, mouse and rat versions of the protein (1,35,36), residues 18-21 (IGGL), residues 23-34 (IAGILFILGILI) and residues 36-37 (LS). Val22 is mutated to Thr in mouse and rat, and to Ile in canine species whilst Val35 is maintained in canine and mutated to Ile in mouse and rat. In our model the residues Ile18, Gly19 and Gly20 all point outwards toward the lipid environment and therefore do not form inter-helical interactions, however the Leu21 residues are in the interior of the α -helical complex and appear to pack uniformly. The Leu36 and Ser37 residues protrude outwards into the surrounding environment, however this region is in the water phase. In the 23-34 residue region; the Gly25, Phe28 and Ile32 residues form the inter-helical binding motif. Perhaps surprisingly, only one glycine residue packs in the interior of the complex while all others point outwards into the lipid environment. One possible explanation is that this arrangement allows PLM to interact with other transmembrane proteins e.g. the Na⁺/K⁺-ATPase. Of the non-conserved residues, Val22 and Val35 are in the interfacial region. In our PLM model, the Phe28 residues reside in the interior of the complex. Interestingly, previous

experimental cross-linking studies of the related γ -subunit identified a Phe residue that was in close proximity to neighbouring helices of the Na⁺/K⁺-ATPase (6). Also Leu42 and Ile43 were identified from modelling studies (in the γ -subunit) to be close to other helices in this complex. These residues are conserved in PLM (as Leu33 and Ile34). In the PLM model presented here, both these residues protrude into the lipid environment. The biological consequences of these findings are that even in its oligomeric form PLM would be able to interact with the Na⁺/K⁺-ATPase, either by stable interaction of the whole PLM tetramer or by forming an intermediate complex from which a PLM monomer is abstracted leaving behind a trimer.

Two-stage model of PLM-Na⁺/K⁺-ATPase interaction – Based on the structure obtained in this report and earlier investigations (19) we present a model of interaction between PLM and the Na⁺/K⁺-ATPase that involves a transient intermediate complex between the PLM tetramer and the Na⁺/K⁺-ATPase. This interaction provides the energy to strip out a subunit of the tetramer in a slow process followed by a fast step of association between the remaining PLM trimer and surrounding Na⁺/K⁺-ATPase molecules (figure 4). The molecular surface of the PLM tetramer presents a hole at the positions Gly19, Gly20 (figure 4A), which would enable PLM to pack closely against other transmembrane helices in this region. On the other hand Leu33 and Ile34 are pointing to the outside of the PLM tetramer and those residues are believed to be in close proximity to the Na⁺/K⁺-ATPase transmembrane helices (in the related γ -subunit (6)). Thus we postulate that the PLM tetramer is able to interact with the Na⁺/K⁺-ATPase at a groove formed by M2, M6 and M9 transmembrane helices (figure 4B). Also the Phe28 was identified by cross linking experiments (in the related γ -subunit) to be in close proximity to the Na⁺/K⁺-ATPase, while our PLM tetramer model would not allow the formation of cross links to other residues of interacting transmembrane helices. Phe28 in our model is buried in the interior of the helical bundle (figure 3C). Thus we must postulate either a conformational change or the dissociation of a PLM trimer from the ATPase/PLM tetramer

complex. The latter possibility is supported by the experimental evidence that a PLM monomer co-immunoprecipitates with the ATPase (10). Oligomerisation studies did not show the existence of a PLM trimer (19), thus it would be unstable and readily interact in a second fast stage with other Na⁺/K⁺-ATPase molecules in the lipid membrane (figure 4B). The biological advantage of our model is a very responsive mode of control of the Na⁺/K⁺-ATPase by PLM reminiscent of a positive-cooperative effect. Once PLM-ATPase interaction has been initiated, by a mechanisms which remain to be investigated, PLM interacts fast and efficiently with ATPase molecules in the surroundings, which is facilitated by clustering of the Na⁺/K⁺-ATPase molecules observed by fluorescence microscopy and immunogold electron microscopy (37).

PLM as a hydrophilic channel – The possibility of the formation of a hydrophilic channel by PLM for ions or taurine has been discussed in the literature (16-18). Visual analysis of the experimentally obtained PLM model shows that, no noticeable cavity exists, and certainly not one that would accommodate a taurine molecule which has a diameter of >2.2Å (38,39) (also shown in figure 3D for comparison). There are strong interactions between various residues occluding the central pore of the tetramer, thus we believe that any conformational change to an open pore would require major structural rearrangements and disruption of inter-residue interactions, which are incompatible with the typical delicate balance between open-close conformations in voltage- or ligand-gated transmembrane channels. However, it

has been shown that hyperpolarisation activates anion currents through PLM (40) and based on further experiments with embryonic kidney cells it has been hypothesised that PLM may facilitate osmolyte influx in renal tissue (18). Indeed, the clustering of four negative charges at the extracellular entrance would provide a binding site for the zwitterionic osmolyte taurine. In order to explore other possible packing models of PLM not encountered in the ATR-FTIR experiments, we performed an unconstrained MD conformational search. Among nine packing models, the lowest energy structure 4 shows a narrow central pore, which is only occluded by the Val34 residue. While structure 4 clearly shows a closed pore, the energy barrier for a conformational transition to an open pore might be overcome by voltage gating or binding of a ligand to the PLM molecule. We predict that mutation of Val34, e.g. Val34Gly, could abolish the gating behaviour and lead to a permanently open channel. This should be explored with further electrophysiology experiments using kidney cells as well as PLM transmembrane peptides in artificial lipid bilayer systems.

In summary, the first experimental high resolution structural investigation of PLM gives credence to the hypothesis of a PLM tetramer as an inactive storage form that nevertheless allows very efficient regulation the Na⁺/K⁺-ATPase in a process reminiscent of a positive-cooperative effect. An experimentally unconstrained modelling study identified another model of biological significance forming a potential closed conformation of a transmembrane channel.

REFERENCES

1. Sweadner, K. J., and Rael, E. (2000) *Genomics* **68**(1), 41-56
2. Palmer, C. J., Scott, B. T., and Jones, L. R. (1991) *J Biol Chem* **266**, 11126-11130
3. Geering, K. (2005) *Journal of Bioenergetics and Biomembranes* **37**(6), 387-392
4. Garty, H., and Karlish, S. J. D. (2006) *Annual Review of Physiology* **68**, 431-459
5. Geering, K. (2001) *J Bioenerg Biomembr* **33**(5), 425-438
6. Lindzen, M., Gottschalk, K. E., Fuzesi, M., Garty, H., and Karlish, S. J. D. (2006) *J. Biol. Chem.* **281**(9), 5947-5955
7. Fuzesi, M., Gottschalk, K. E., Lindzen, M., Shainskaya, A., and Kuster, B. (2005) *J. Biol. Chem.* **280**, 18291-19301

8. Mounsey, J. P., Lu, K. P., Patel, M. K., Chen, Z. H., Horne, L. T., John, J. E., 3rd, Means, A. R., Jones, L. R., and Moorman, J. R. (1999) *Biochim Biophys Acta* **1451**(2-3), 305-318
9. Zhang, X. Q., Ahlers, B. A., Tucker, A. L., Song, J., Wang, J., Moorman, J. R., Mounsey, J. P., Carl, L. L., Rothblum, L. I., and Cheung, J. Y. (2006) *J Biol Chem* **281**(12), 7784-7792
10. Ahlers, B. A., Zhang, X. Q., Moorman, J. R., Rothblum, L. I., Carl, L. L., Song, J., Wang, J., Geddis, L. M., Tucker, A. L., Mounsey, J. P., and Cheung, J. Y. (2005) *J Biol Chem* **280**(20), 19875-19882
11. Jia, L. G., Donnet, C., Bogaev, R. C., Blatt, R. J., McKinney, C. E., Day, K. H., Berr, S. S., Jones, L. R., Moorman, J. R., Sweadner, K. J., and Tucker, A. L. (2005) *Am J Physiol Heart Circ Physiol* **288**(4), H1982-1988
12. Song, J., Zhang, X. Q., Ahlers, B. A., Carl, L. L., Wang, J., Rothblum, L. I., Stahl, R. C., Mounsey, J. P., Tucker, A. L., Moorman, J. R., and Cheung, J. Y. (2005) *Am J Physiol Heart Circ Physiol*
13. Zhang, X. Q., Qureshi, A., Song, J., Carl, L. L., Tian, Q., Stahl, R. C., Carey, D. J., Rothblum, L. I., and Cheung, J. Y. (2003) *Am J Physiol Heart Circ Physiol* **284**(1), H225-233
14. Despa, S., Bossuyt, J., Han, F., Ginsburg, K. S., Jia, L. G., Kutchai, H., Tucker, A. L., and Bers, D. M. (2005) *Circ Res* **97**(3), 252-259
15. Silverman, B. Z., Fuller, W., Eaton, P., Deng, J., Moorman, J. R., Cheung, J. Y., James, A. F., and Shattock, M. J. (2005) *Cardiovascular Research* **65**(1), 93-103
16. Chen, Z.-H., Jones, L. R., and Moorman, J. R. (1999) *Receptors and Channels* **6**, 435-447
17. Moorman, J. R., and Jones, L. R. (1998) *Adv. Exp. Med. Biol.* **442**, 219-228
18. Davis, C. E., Patel, M. K., Miller, J. R., John, J. E., 3rd, Jones, L. R., Tucker, A. L., Mounsey, J. P., and Moorman, J. R. (2004) *Neurochem Res* **29**(1), 177-187
19. Beevers, A. J., and Kukol, A. (2006) *Protein Science* **15**, 1127-1132
20. Chen, Z., Jones, L. R., O'Brian, J. J., Moorman, J. R., and Cala, S. E. (1998) *Circ Res* **82**(3), 367-374
21. Kukol, A., Adams, P. D., Rice, L. M., Brunger, A. T., and Arkin, I. T. (1999) *J. Mol. Biol.* **286**, 951-962
22. Kukol, A. (2005) *Spectroscopy* **19**, 1-16
23. Beevers, A. J., and Kukol, A. (2006) *J Mol Graph Model* **25**(2), 226-233
24. Beevers, A. J., and Kukol, A. (2006) *J. Mol. Biol.* **361**(5), 945-953
25. Torres, J., Adams, P. D., and Arkin, I. T. (2000) *J. Mol. Biol.* **300**, 677-685
26. Torres, J., Kukol, A., Goodman, J. M., and Arkin, I. T. (2001) *Biopolymers* **59**, 396-401
27. Kortenaar, P. B. W., Van Dijk, B. G., Peeters, J. M., Raaben, B. J., Adams, P. J. H. M., and Tesser, G. I. (1986) *International Journal of Peptide and Protein Research* **27**, 398-400
28. Kass, I., Arbely, E., and Arkin, I. T. (2004) *Biophys. J.* **86**, 2502-2507
29. Arkin, I. T., MacKenzie, K. R., and Brünger, A. T. (1997) *Journal of the American Chemical Society* **119**(38), 8973-8980
30. Marsh, D., Muller, M., and Schmitt, F. J. (2000) *Biophys J* **78**(5), 2499-2510
31. Lindahl, E., Hess, B., and van der Spoel, D. (2001) *J. Mol. Mod.* **7**, 306-317
32. Gurtovenko, A. A., Patra, M., Karrttunen, M., and Vattulainen, I. (2004) *Biophys. J.* **86**, 3461-3472
33. Byler, D. M., and Susi, H. (1986) *Biopolymers* **25**, 469-487

34. Kukol, A., and Arkin, I. T. (1999) *Biophys. J.* **77**, 1594-1601
35. Altschul, S. F., Madden, T. L., Schaffer, A. A., Zhang, J., Zhang, Z., Miller, W., and Lipman, D. J. (1997) *Nucleic Acids Research* **25**, 3389-3402
36. Bogaev, R. C., Jia, L., Kobayashi, Y. M., Palmer, C. J., Mounsey, J. P., Moorman, J. R., Jones, L. R., and Tucker, A. L. (2001) *Gene* **271**, 69-79
37. Dalskov, S. M., Immerdal, L., Niels-Christiansen, L. L., Hansen, G. H., Schousboe, A., and Danielsen, E. M. (2005) *Neurochem Int* **46**(6), 489-499
38. Allen, F. H. (2002) *Acta Crystallographa* **B58**, 380-388
39. Fletcher, D. A., McMeeking, R. F., and Parkin, D. J. (1996) *Journal of Chem. Inf. Comput. Sci.* **36**, 746-749
40. Moorman, J. R., Ackerman, S. J., Kowdley, G. C., Griffin, M. P., Mounsey, J. P., Chen, Z., Cala, S. E., O'Brian, J. J., Szabo, G., and Jones, L. R. (1995) *Nature* **377**(6551), 737-740
41. Humphrey, W., Dalke, A., and Schulten, K. (1996) *Journal of Molecular Graphics* **14**(1), 33-38

FOOTNOTES

*We would like to express our thanks to Sue Slade, Charlotte Winn and Sarah Nicholson of the University of Warwick Proteomics group for mass spectrometry analysis and to Dr. Teresa Pinheiro for generous access to the FTIR spectrometer, which was funded by the Medical Research Council UK (grant no. G9901445). This work was funded by the Biotechnology and Biological Sciences Research Council UK (grant no. 88/B19450).

The abbreviations used are: PLM, phospholemman; ATR-FTIR, attenuated total reflection Fourier-transform infrared; SSID, site-specific infrared dichroism; MD, molecular dynamics; RMSD, root mean square deviation.

FIGURE LEGENDS

Figure 1: Infrared spectra for each peptide containing a $^{13}\text{C}^{18}\text{O}$ label in the position indicated in the top right. The amide I area is displayed, while the insert shows the magnified amide I absorption band of the label.

Figure 2: (A) Polar plot of the energies of structures obtained from MD simulation of PLM in dependence of the helix rotation angle ϕ changing clockwise from 0° to 360° . The distance from the centre indicates negative energy (E) in kJ/mol. Each individual structure is indicated by a triangle, while the clustered averages are shown as numbered circles. The arcs represent the movement of structures from their starting positions with respect to the helix rotation angle ϕ during the MD simulation. (B) The rotation of the helix tetramer defined as $\phi=0$, Phe28 residues shown in wireframe.

Figure 3: Resulting structure (structure 6) from MD simulation. (A) Showing the α -helical bundle in a lipid bilayer. (B) Spacefill rendering with labelled residues shown in black. (C) Positions of the Phe28 residues in this model viewed from the top (the direction of the membrane normal). (D) Spacefill rendering of the model viewed from the top and a relative comparison to the size of a taurine molecule. All images were created using the VMD molecular rendering software (41).

Phospholemman Transmembrane Structure

Figure 4: (A) A surface rendering of the PLM tetramer model indicating residues in spacefill representation that would facilitate interaction between the PLM tetramer and the Na^+/K^+ -ATPase. (B) The two stage model of the control of Na^+/K^+ -ATPase by PLM tetramers. The PLM transmembrane helices are shaded in dark grey, while the Na^+/K^+ -ATPase molecules are represented schematically in light grey. The view is in the direction of the cell membrane normal axis. Please note that the shape of the Na^+/K^+ -ATPase is drawn arbitrarily and that no indication of the relative location of PLM and ATPase is implicated.

Figure 5: (A) Polar plot of the energies of structures obtained from MD simulation of PLM in dependence of the helix rotation angle ϕ changing clockwise from 0° to 360° . The distance from the centre indicates negative energy (E) in kJ/mol. Each individual structure is indicated by a triangle, while the cluster average structures are shown as numbered circles. The arcs represent the movement of structures from their starting positions with respect to the helix rotation angle ϕ during the MD simulation. (B) Lowest energy structure 4 with pore-occluding residues Tyr27 and Val34 rendered in spacefill representation.

Table I: Experimentally determined orientations: rotational pitch angle ω , local tilt angle β and the derived angle of the carbonyl bond to the z-axis θ for all labels in the transmembrane domain – calculated from the SSID data. Standard errors are $\beta \pm 4^\circ$ and $\omega \pm 20^\circ$.

Label	β	ω	θ
G20	8.9°	64°	40.2°
L21	8.3°	119°	44.3°
V22	4.9°	235°	36.8°
I23	8.8°	327°	46.6°
G25	8.7°	206°	32.0°
I26	10.1°	302°	46.0°
L27	6.2°	15°	43.4°
G31	2.5°	213°	36.4°
I32	7.3°	298°	43.4°

Table II: Comparison of rotational pitch angles from SSID with the structures produced from the MD search: ω_{exp} denotes the experimental rotational pitch angle, while ω_{model} is the angle calculated from the computational model. The deviation between the MD simulated structures and the experimental data is also shown. This has been calculated using the equation

$$\sqrt{\sum (\omega_{\text{exp}} - \omega_{\text{model}})^2}$$

Label	ω_{exp}	ω_{model}^1	ω_{model}^2	ω_{model}^3	ω_{model}^4	ω_{model}^5	ω_{model}^6
G20	64°	57°	259°	322°	10°	203°	313°
L21	119°	243°	341°	52°	71°	340°	27°
V22	235°	334°	92°	160°	172°	31°	126°
I23	327°	46°	200°	352°	301°	240°	304°
G25	206°	347°	49°	23°	121°	147°	177°
I26	302°	294°	355°	151°	9°	338°	315°
L27	15°	352°	19°	10°	21°	54°	62°
G31	213°	168°	108°	117°	85°	154°	156°
I32	298°	271°	250°	279°	207°	262°	248°
Deviation		1069	1054	879	794	880	669

FIGURE 1

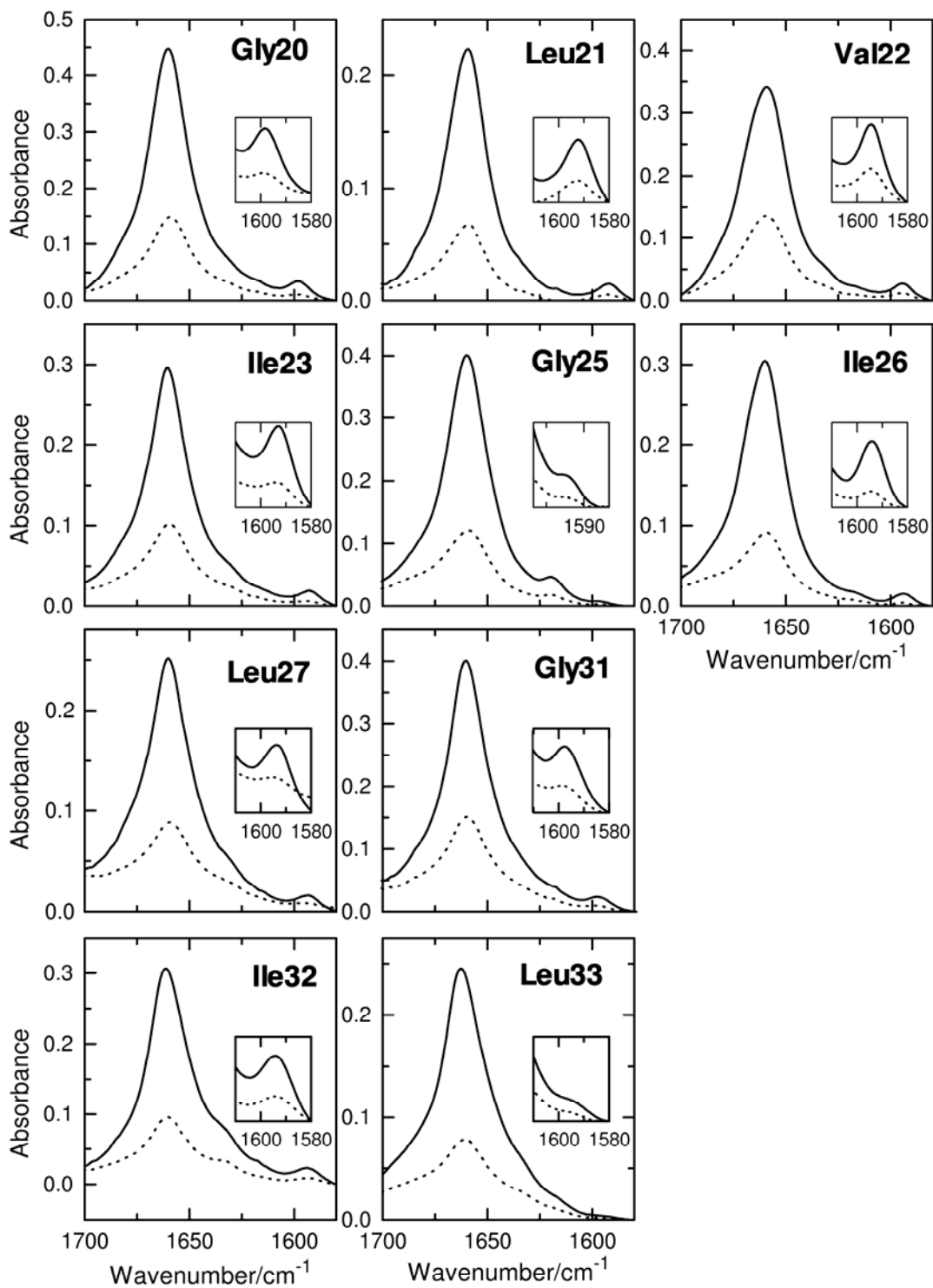


FIGURE 2

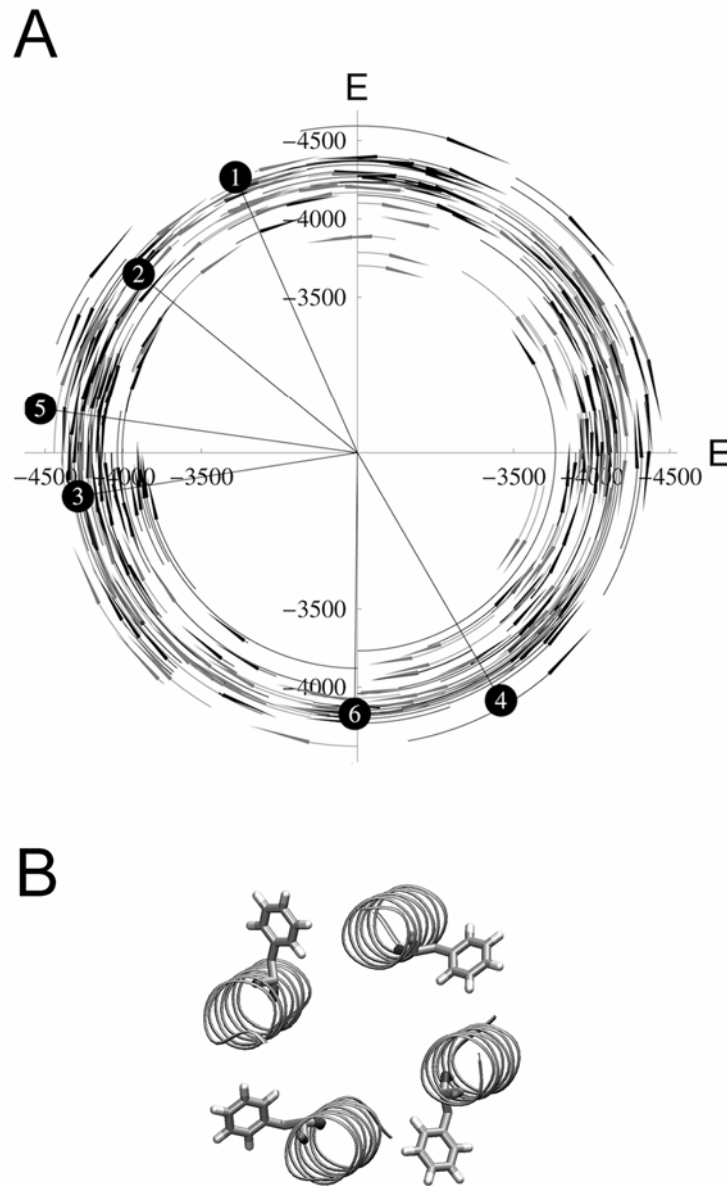


FIGURE 3

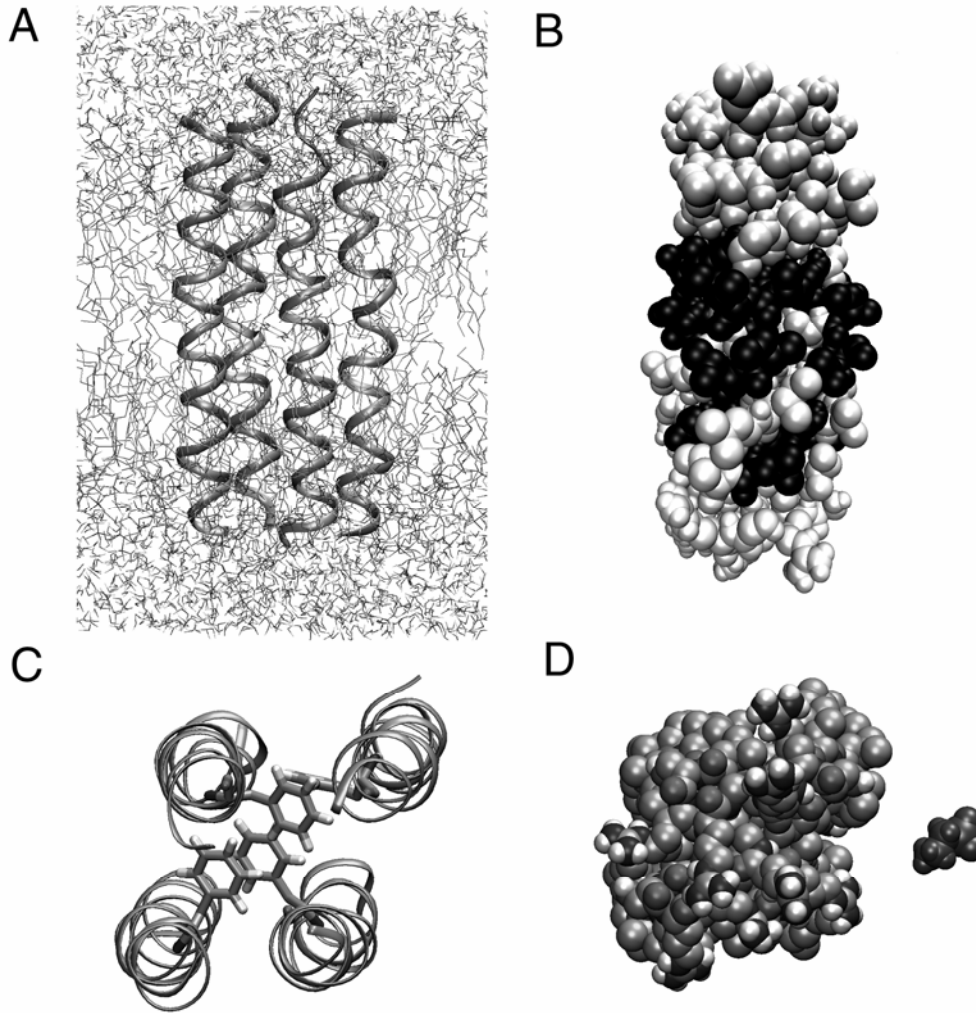


FIGURE 4

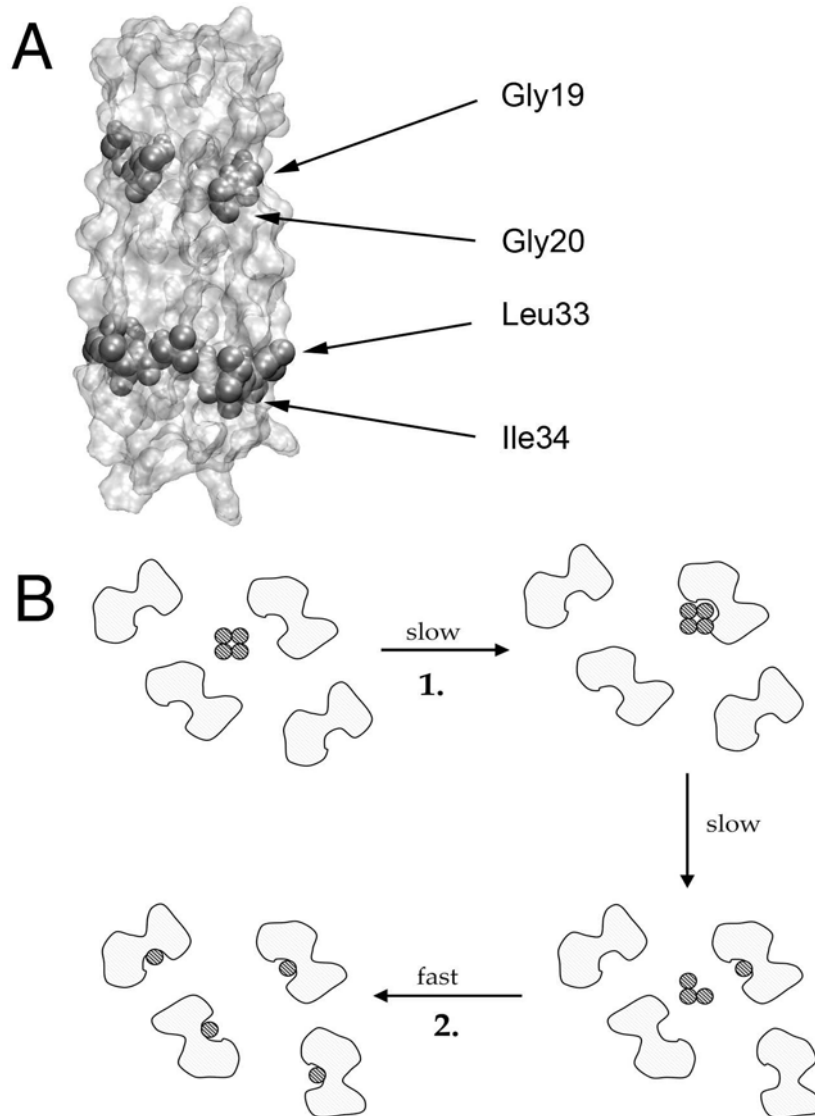


FIGURE 5

